Received 25 April 2024; Accepted 19 May 2024
https://doi.org/10.48612/letters/2024-3-175-182
https://elibrary.ru/bzarbo

Elasticity of pentagonal wires: single disclination model versus distributed disclination model

R. E. Shevchuk[1], S. A. Krasnitckii[1], A. E. Romanov[1,2,3], A. M. Smirnov[†1]

[†]smirnov.mech@gmail.com

[1]ITMO University, St. Petersburg 197101, Russia
[2]Ioffe Institute, St. Petersburg 194021, Russia
[3]Togliatti State University, Togliatti 445020, Russia

Abstract: Elasticity of pentagonal wires is analyzed in the framework of distributed disclination model. According to this model, the elastic field induced by five-fold cyclic twinning in pentagonal wires is treated as generated by a distributed disclination with uniform angular eigenstrain. Originally, the concept of distributed disclination was introduced by Howie and Marks to describe the stress-strain state of icosahedral particles in terms of the so-called Marks-Yoffe stereo-disclination. Differences between the proposed distributed disclination model and standard single disclination model are examined by an analytical technique and the finite element method. In doing so, the distribution of displacement vector and stress tensor components in pentagonal wires, as well as the dependencies of strain energy on the Poisson's ratio of pentagonal wires, are analyzed. Analytical investigation demonstrates that both models prescribe the same expressions for mechanical stresses and strain energy, while the expressions for displacement components differ because of the plastic rotation inherent to wedge disclinations. Parametric finite element simulations are employed to estimate the accuracy of circular cross-section approximation used in both the single disclination and distributed disclination analytical models. It is demonstrated that the discrepancy between analytical results for cylindrical wires and results of finite element computations for faceted wires is ≈5%. Besides, the finite element modeling of distributed disclination allows one to obtain the desired solution with less computational resources.

Keywords: disclination, multiply twinned particles, single disclination model, distributed disclination model

Acknowledgments: *The study was supported by the Russian Science Foundation, project No 23-72-10014.*

1. Introduction

Unique functional properties of multiply twinned particles of fcc metals determine their applicability in various fields of modern nanotechnologies, e. g., related to catalysis and plasmonics [1–4]. The main attributes of the intrinsic structure of these particles are predominantly external faceting by {111}-type planes and internal cyclic twinning, which enhance their performance in comparison to single- and polycrystalline counterparts [5–8]. The cyclic twinning is also responsible for inhomogeneous mechanical stress inside the particles, provoking the storage of a significant amount of strain energy [9,10]. This energy has a tendency to relieve through different mechanisms of structural degradation such as dislocation formation [11–14], pore nucleation [15–18], etc. A control of structural defects to maintain the stability of multiply twinned particles can be achieved with the help of a thorough analysis of their inhomogeneous stresses.

The stress-strain state in multiply twinned particles has been long studied experimentally [19–21] and theoretically [22–24]. The experimental research of the intrinsic structure of these particles, provided by high-resolution transmission electron microscopy and geometric phase analysis, clearly indicates a crystal lattice distortion inherent to disclination defects [21]. Theoretical models of disclination defects in multiply twinned particles can be categorized with respect to the way a defect is introduced viz. single [22] and distributed [23] disclination models. The first group of models employs the presence of a positive wedge disclination (WD) to describe the inhomogeneous stress of pentagonal wires (PWs) and decahedral particles, whereas the second one stems from a so-called Marks-Yoffe stereo-disclination (SD) homogeneously distributed over the volume of a particle and is usually applied to icosahedral particles. Such conventional categorization is addressed to the fact that PWs and decahedral particles contain a single WD piercing through their poles while the icosahedral particles contain a configuration of six positive WDs passing through opposite vertices of the icosahedron. This fact makes it difficult to apply the discrete approach to icosahedral particles mainly because of the absence of a proper theoretical mean such as an interaction energy of the WDs in an elastic finite body [25].

Recently, the energy of pair interaction of intersecting WDs in an elastic spherical body has been theoretically obtained by Kolesnikova et al. [26]. The found solution

allows elucidating the discrepancy between the single and distributed disclination models of icosahedral particles. It was demonstrated that the difference between strain energies of the configuration of six WDs and the Marks-Yoffe disclination strongly depends on Poisson's ratio ν of the particle material. For example, if the material of icosahedral particles is insensitive to Poisson effect ($\nu = 0$), the strain energy of Marks-Yoffe disclination is ≈2.5 times less than the one corresponding to six WDs. In the case of incompressible material ($\nu = 0.5$), the ratio of these strain energies is estimated as ≈1.4. Similar calculations have not been extended to PWs and decahedral particles yet. Therefore, the comparative analysis of single and distributed disclination models of these pentagonal particles is considered a significant issue in the disclination concept to investigate.

Another challenging issue of the disclination concept is the necessity to incorporate the external faceting of multiply twinned particles in theoretical modelling. The aforementioned analytical models treat these particles either as cylindrical [11,17] or spherical [12,16] bodies, so they are unable to consider the impact of the polyhedral shape on stress concentration effect in spite of the well-known fact that this effect is responsible for dislocation formation in the vicinity of polyhedral edges of core-shell nanoparticles with multiply twinned structures [27–29]. This limitation can be surmounted in the frame of numerical techniques viz. finite element method and molecular dynamic simulation.

The finite element (FE) method, as one of the effective tools, is applicable for the description of stress-strain state in objects with complex geometry such as multiply twinned particles, in particular. Patala et al. [30,31] calculate the strain energy of elastically anisotropic decahedral and icosahedral particles within finite element simulations to investigate the morphological relaxation due to the formation of re-entrant external faceting. As for molecular dynamic studies, the simulations concern various structural aspects of disclination defects located in a circular plate [32], nanowires [33,34], and icosahedral particles [35,36], polycrystalline bulk materials [37,38], and two-dimensional materials such as graphene, pseudo-graphenes [39], and phosphorene [40].

Encouraged by the recently revealed difference in strain energies determined within single and distributed disclination models of icosahedral particles [26], the present work aims to provide a comprehensive analysis of the single and distributed disclination models of PWs. In doing so, a new distributed disclination model of PWs is derived analytically and then simulated by FE methods, taking into account the actual PW shape. The FE outputs are verified by the obtained analytical solution. The discrepancy between elastic fields and strain energy prescribed by single and distributed disclination models of the PWs is discussed in detail.

2. Theoretical models

Consider a cross-section of the PW with a fcc crystal structure composed of five triangle prisms with lateral faces of {100}-type crystallographic planes as it is illustrated in Fig. 1a. These prisms assemble about the common edge with <110>-type crystallographic direction forming twin boundaries between adjoining faces. The complete space-filling of such twinned structure can be accomplished by suggesting the occurrence of an internal elastic distortion.

This internal distortion in PWs can be understood within the disclination concept. According to this concept, the PW is treated as an elastic cylinder containing an positive WD of strength $\omega \approx 0.128$ [22]. Figure 1b demonstrates the Volterra procedure for an elastic cylinder with a missing sector ω with the verges loaded by internal forces to provide its continuity. The obtained jump of tangential displacement at the cut $[u_\varphi] = \omega r$ is responsible for the elastic disturbance in the cylinder. The well-known elastic fields of the WD in an infinite elastically isotropic cylinder are given in [22]. The non-zero displacement components are described by the equations:

$$u_r = \frac{\omega r}{4\pi}\left(\frac{1-2\nu}{1-\nu}\ln\frac{r}{R_0} - 1\right), \tag{1}$$

$$u_\varphi = \frac{\omega r \varphi}{2\pi}, \tag{2}$$

and the non-zero stress tensor components are found in the form:

$$\sigma_{rr} = \frac{G\omega}{2\pi(1-\nu)}\ln\frac{r}{R_0}, \tag{3}$$

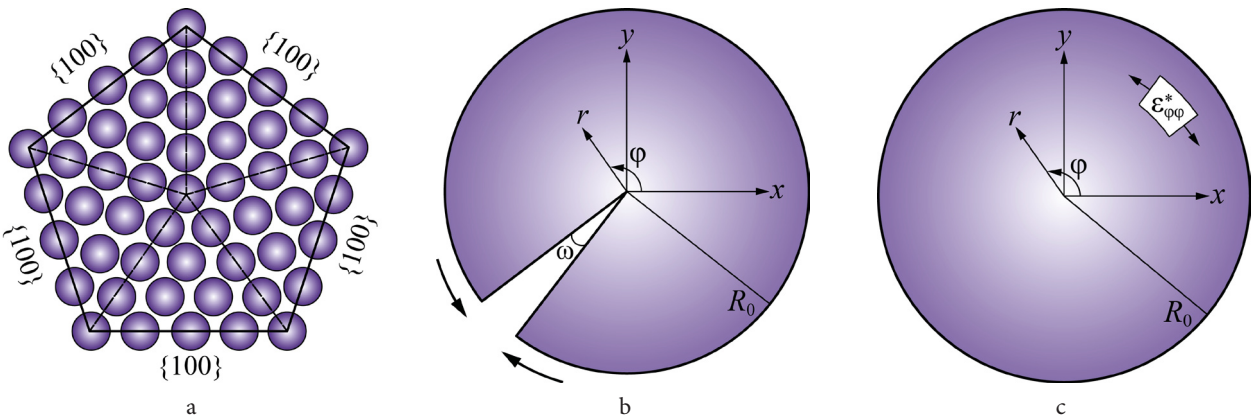

Fig. 1. (Color online) The cross-section of the actual PW (a); the elastic cylinder with a missing sector $\omega \approx 0.128$ related to the positive WD as a single disclination model of PW (b); SD with eigenstrain $\varepsilon^*_{\varphi\varphi} = \omega/[2\pi]$ in the elastic cylinder as a distributed disclination model of PW (c).

$$\sigma_{\varphi\varphi} = \frac{G\omega}{2\pi(1-\nu)}\left(1+\ln\frac{r}{R_0}\right), \quad (4)$$

$$\sigma_{zz} = \frac{\nu G\omega}{2\pi(1-\nu)}\left(1+2\ln\frac{r}{R_0}\right), \quad (5)$$

where (r, φ, z) is the cylindrical coordinate system associated with the cylinder axis, R_0 is this cylinder radius, G is the shear modulus of the material and ν is the Poisson's ratio. The strain energy stored in the disclinated elastic cylinder is [22]

$$E_{st} = \frac{G\omega^2 R_0^2}{16\pi(1-\nu)}. \quad (6)$$

The elastic field induced by the WD in the PW hereinafter is referred as related to a single disclination model of the PW.

As it was mentioned in the introduction section, the alternative approach to define the elastic distortion of the multiplied twinned particles was suggested by Howie and Marks for the case of icosahedral particles [23]. According to this approach, the elastic field in the particle is caused by the distributed disclination or the so-called Marks-Yoffe SD with tangential eigenstrain spread uniformly over the particle volume $\varepsilon^*_{\varphi\varphi} = \varepsilon^*_{\theta\theta} = 6\omega/[4\pi] \approx 0.061$ (here θ and φ are the polar and azimuthal angles of the associated spherical coordinate system, respectively). This eigenstrain state arises from the particle volume change ≈12% attributed to the missing volume between 20 tetrahedral domains with faces of {111}-type put together to form a solid icosahedron.

As for PWs, the similar SD exerting the tangential eigenstrain $\varepsilon^*_{\varphi\varphi} = \omega/[2\pi] \approx 0.02$ over the elastic cylinder produces the angular deficiency corresponding to the internal distortion of the cycling twinning (see Fig. 1c). Alternatively, one can treat this SD as a superposition of WDs with infinitesimally small strength $d\omega$ uniformly distributed over the cylinder. Hereinafter, the introduced internal distortion in PW is addressed as a distributed disclination model of the PW.

The elastic fields in a PW within the distributed disclination model can be determined by integration of the equations of equilibrium for the cylinder with the prescribed eigenstrain. Taking into consideration the cylindrical symmetry, one can assume that the radial displacement u_r only depends on the polar radius r. For the tangential displacement of the axisymmetrically loaded body, it is valid that $u_\varphi = 0$. Hence, the radial and tangential strains can be cast as follows

$$\varepsilon_{rr} = \frac{du_r}{dr}, \quad (7)$$

$$\varepsilon_{\varphi\varphi} = \frac{u_r}{r}. \quad (8)$$

As for axial strain, the generalized plane strain condition with $\varepsilon_{zz} = \text{const}$ is presumed.

The Hooke's law accounting for the tangential eigenstrain $\varepsilon^*_{\varphi\varphi} = \omega/[2\pi]$ can be written

$$\sigma_{rr} = 2G\left[\varepsilon_{rr} + \frac{\nu}{1-2\nu}\Delta - \frac{\nu}{1-2\nu}\frac{\omega}{2\pi}\right], \quad (9)$$

$$\sigma_{\varphi\varphi} = 2G\left[\varepsilon_{\varphi\varphi} + \frac{\nu}{1-2\nu}\Delta - \frac{1-\nu}{1-2\nu}\frac{\omega}{2\pi}\right], \quad (10)$$

$$\sigma_{zz} = 2G\left[\varepsilon_{zz} + \frac{\nu}{1-2\nu}\Delta - \frac{\nu}{1-2\nu}\frac{\omega}{2\pi}\right], \quad (11)$$

where $\Delta = \varepsilon_{rr} + \varepsilon_{\varphi\varphi} + \varepsilon_{zz}$ is the dilatation.

Substituting Eqs. (7)–(11) in the only non-zero equilibrium equation:

$$\frac{d\sigma_{rr}}{dr} + \frac{\sigma_{rr} - \sigma_{\varphi\varphi}}{r} = 0, \quad (12)$$

finally, one can obtain the following differential equation for radial displacement:

$$\frac{d^2u_r}{dr^2} + \frac{1}{r}\frac{du_r}{dr} - \frac{u_r}{r^2} + \frac{1-2\nu}{1-\nu}\frac{\omega}{2\pi r} = 0. \quad (13)$$

The solution of Eq. (13) can be presented as

$$u_r = Ar + B\frac{1}{r} + \frac{1-2\nu}{1-\nu}\frac{\omega r}{8\pi}(1-2\ln r), \quad (14)$$

where A and B are the constants of integration determined by the boundary conditions. Since the displacement should take the finite values $u_r(r \to 0) = \text{const}$, the constant B vanishes ($B = 0$) in Eq. (14). The surface of the cylindrical body is presumed to be traction-free, so the condition $\sigma_{rr}(r = R_0) = 0$ gives the expression for constant A:

$$A = \nu\varepsilon_{zz} + \frac{\omega}{8\pi(1-\nu)}\left[\frac{1}{2} + (1-2\nu)\ln R_0\right]. \quad (15)$$

The unknown parameter ε_{zz} in Eq. (15) can be defined in terms of equilibrium of the cylindrical body. The condition of vanishing total resultant axial force $\int_0^{R_0}\sigma_{zz}\,r\,dr = 0$ finally gives:

$$\varepsilon_{zz} = -\frac{\nu\omega}{1-\nu^2}\ln R_0. \quad (16)$$

Taking into account Eqs. (14)–(16) the same expressions for radial displacement (Eq. (1)) and stress tensor components (Eqs. (3)–(5)) can be obtained. As for tangential displacement, it is presumed to take zero values due to the axial symmetry of the SD problem, in contrast to the classical problem of the WD with tangential displacement given by Eq. (2). Thus, the internal distortions of WD and SD produce different displacements despite the fact that the stresses are identical.

As for the specific strain energy stored by SD in the cylinder, it can be found as the work done during the SD formation in its own stress field $\sigma_{\varphi\varphi}$ in the following form:

$$E_{st} = -\frac{1}{2}\int_S \varepsilon^*_{\varphi\varphi}\sigma_{\varphi\varphi}\,dS, \quad (17)$$

where S is the area of PW cross section. Considering Eq. (10) and $dS = r\,dr\,d\varphi$, $\varepsilon^*_{\varphi\varphi} = \omega/[2\pi]$, one can derive the final expression from Eq. (17) for the strain energy of SD identical to the strain energy of WD (see Eq. (6)).

Thus, in the case of the cylindrical approximation of the PW surface, the single and distributed disclination models prescribe the same mechanical stresses and strain energies, whereas their total displacements are different.

3. Finite element modeling

The parametric FE simulations were employed to investigate the elastic response of PWs within the single and distributed disclination approaches. Figures 2 a and b illustrate the FE models prepared in ANSYS Academic Research software

and representing the cross-section of faceting PWs subjected to the local and distributed disclination distortions, respectively. The area of the PW sections is assumed to be equal to that of a circle of radius R_0. The FE mesh implements the plane strain approximation, and it is built up from the plane elements with a quadratic shape function to provide more accurate calculations. The traction-free conditions are defined for mesh nodes at the boundary of the models. Besides, the central node of the FE meshes is fixed to prevent rigid body motion. The behavior of the PW material is elastic and isotropic.

In order to incorporate the local internal distortion attributed to WD in the model made up of five isosceles triangles with vertex angles equal to $\cos^{-1}(1/3)$ (see Fig. 2 a), the nodes placed at the verges of the missing sector get a tangential displacement $\pm\omega r/2$ with subsequent bonding due to the activation of contact elements implementing the bonded-MPC algorithm.

As for the distributed internal distortion induced by SD, the eigenstrain $\varepsilon^*_{\varphi\varphi} = \omega/[2\pi]$ should be injected into the model composed of five isosceles triangles with vertex angles equal to $2\cdot\pi/5$ (see Fig. 2 b). However, almost all modern FE software does not directly implement this option. Such a disadvantage can be overcome by means of the thermal strain analogy. In doing so, the PW material is endowed with orthotropic thermal expansion property with coefficients given in the global cylindrical coordinate system as $\alpha_{rr} = \alpha_{zz} = 0$ and $\alpha_{\varphi\varphi} = \omega/[2\pi]$ K^{-1}. Finally, the increment of nodal temperature $\Delta T = -1$ K is employed to provide the desired eigenstrain $\varepsilon^*_{\varphi\varphi}$.

The FE solutions are demonstrated in Fig. 2 b, c with maps of the total displacement $|\mathbf{u}| = \sqrt{u_r^2 + u_\varphi^2}$ for single and distributed disclination models. As seen from the figures, the pentagonal faceting of PW significantly disturbs the displacement isolines. Additionally, the obvious difference between the distribution of $|\mathbf{u}|$ induced by WD and SD originates from the fact that the internal distortion of WD involves the plastic rotation of verges of the missing gap. Moreover, the mode of incorporation of the distortion in the FE model can essentially impact the theoretical estimation of the elastic fields and strain energy as well. In the next section the discrepancy between the numerical and analytical modeling of the elastic response of the PWs is discussed in detail.

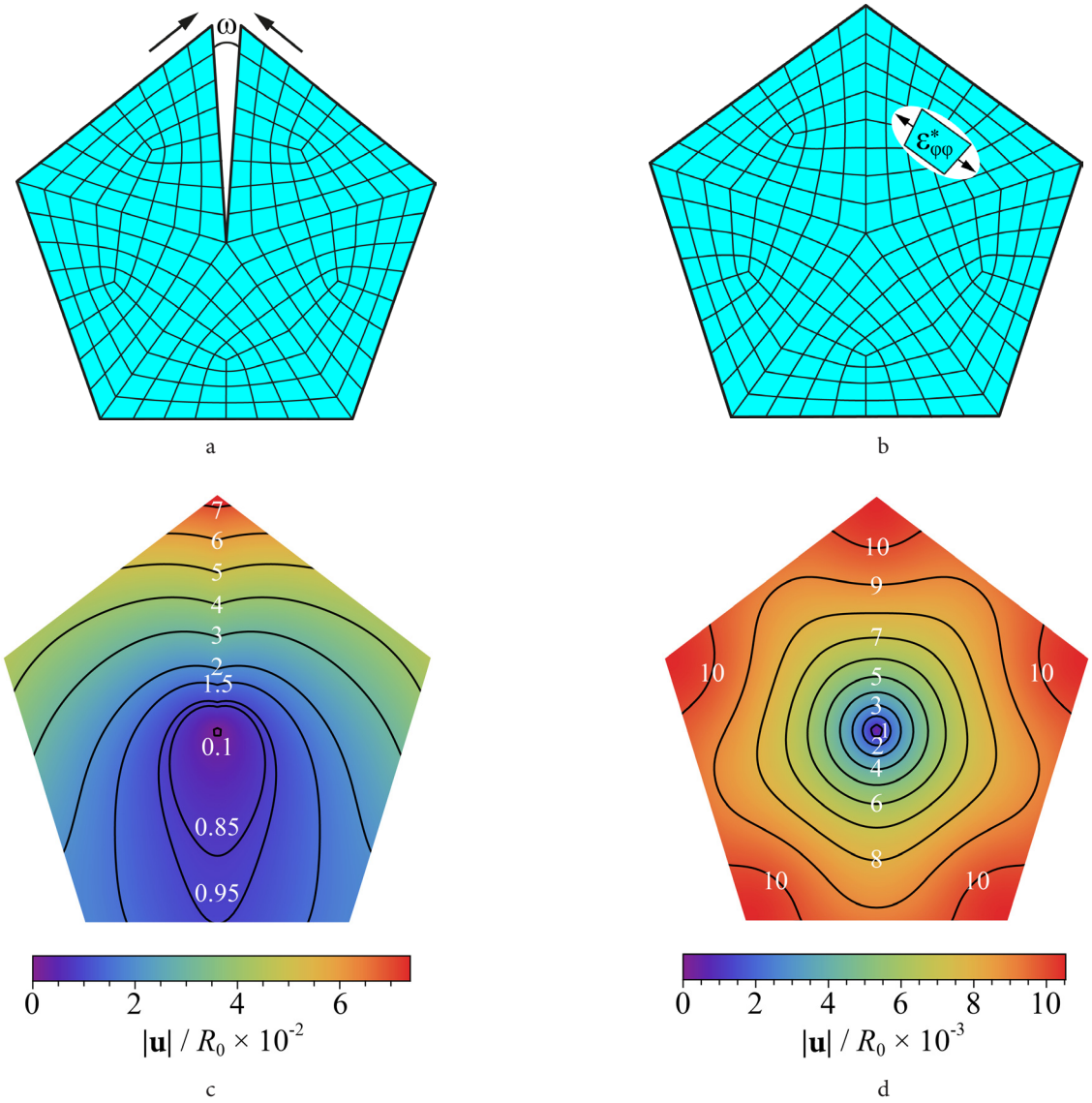

Fig. 2. (Color online) The FE meshes (a), (b) and the FE total displacement $|\mathbf{u}|$ (c), (d) in the PW cross-section are given for $\nu = 0.25$. Figures (a) and (c) refer to single disclination models, while (b) and (d) refer to distributed disclination models. R_0 is the radius of a circle with an area equal to the pentagonal one.

4. Results and discussion

This section is devoted to the analysis of the contribution of the actual faceting of PWs and the mode of internal distortion to the accuracy of theoretical modeling. The following analytical and numerical solutions are considered:

(i) analytical dependencies of the WD elastic fields in the cylindrical body as a single disclination model of PWs;

(ii) analytical dependencies of the SD elastic fields in the cylindrical body as a distributed disclination model of PWs;

(iii) numerical computations of the WD elastic fields in the pentagonal prism as a single disclination model of faceting PWs;

(iv) numerical computations of the SD elastic fields in the pentagonal prism as a distributed disclination model of faceting PWs.

The radial and tangential displacement provided by the single and distributed disclination models within analytical and numerical approaches are illustrated in Fig. 3 a and b, respectively. As seen from Fig. 3 a, analytical curves and numerical data demonstrate similar behavior viz. the ratio r/R_0 increase is accompanied by decrease in u_r. The FE radial displacements along pentagon circumradius (OA) induced by both WD and SD take values less than the ones prescribed analytically for a cylinder. Additionally, the displacements obtained numerically for OA almost coincide. In case of WD, the FE radial displacement along the pentagon apothems (OB) exceeds the analytical curves, while for SD it is inferior.

Figure 3 b depicts the dependencies of tangential displacement on the polar angle $\varphi - \pi/2$ given for the points located at the body boundaries. As shown, the numerical data verify the analytical solutions for both WD and SD.

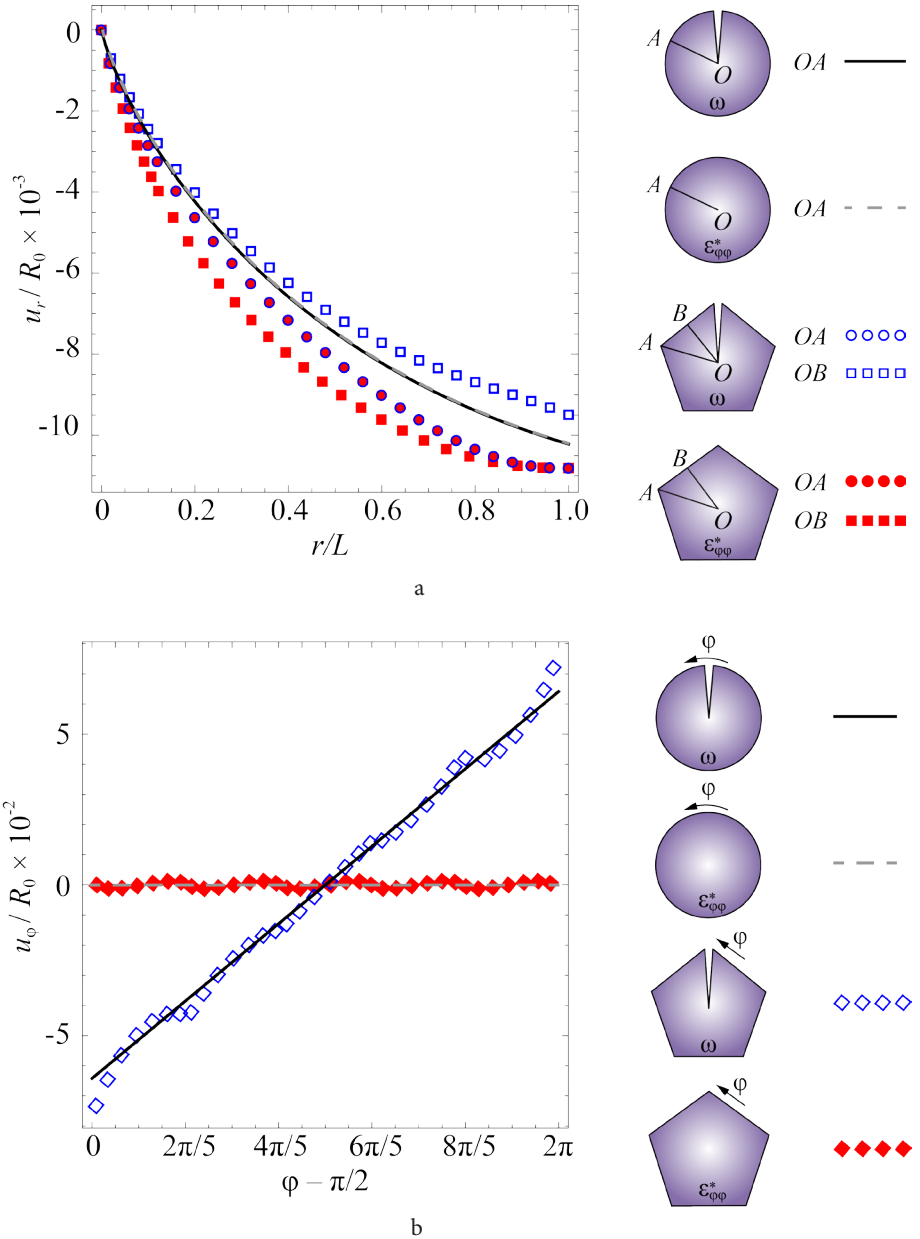

Fig. 3. (Color online) Dependencies of the displacement components induced by a disclination defect: u_r on the normalized radial distance r/L ($L = R_0$ for the cylinder, $L = OA$ for the pentagon circumradius and $L = OB$ for the pentagon apothem) (a), and u_φ at the free boundary of the bodies on the angle $\varphi - \pi/2$ (b). The displacement in the PWs is given for the analytical (solid and dashed curves correspond to single and distributed disclinations respectively) and the FE solutions (marks) for $\nu = 0.25$.

Moreover, the validity of the axial-symmetry assumption in the case of SD is confirmed. As for WD, the FE tangential displacement in a pentagonal body depends linearly on the angular coordinate, as claimed by analytics for a cylindrical one.

Figures 4 a, b and c illustrate the dependencies of the stress tensor components σ_{rr}, $\sigma_{\varphi\varphi}$ and σ_{zz} on the ratio r/L ($L=R_0$ for a cylinder, $L\approx1.15R_0$ for the pentagon circumradius OA, and $L\approx0.93R_0$ for the pentagon apothem OB). As seen from the figures, the numerical data are in good agreement with analytical solutions, particularly for the region with $r<0.7R_0$. The biggest discrepancy between the models is observed in the peripheral area ($r>0.7R_0$). It is worth noting that stresses $\sigma_{\varphi\varphi}$ and σ_{zz} obtained numerically for WD and SD along the circumradius (OA) of the pentagon take values less than those obtained analytically for a cylinder. Hence, the pentagonal shape of actual PWs is responsible for stress relaxation in the vicinity of their edges.

The obtained FE data allow one to calculate the strain energy induced by WD and SD in a pentagonal body as

$$E_{st}=\frac{1}{2}\sum_{n=1}^{N_{el}}S_n\sigma_{ij}^{(n)}\varepsilon_{ij}^{(n)}, \qquad (18)$$

where N_{el} is the number of elements in the model, S_n is the area of the n-th element, $\sigma_{ij}^{(n)}$ and $\varepsilon_{ij}^{(n)}$ are the stress and strain tensor components corresponding to the n-th element. Figure 4 d demonstrates the energy curves $E_{st}(\nu)$ determined analytically by Eq. (6) and numerically by Eq. (18) for the case of equal areas of the pentagonal and cylindrical sections. As shown in Fig. 4 d, the strain energy rises with Poisson's ratio

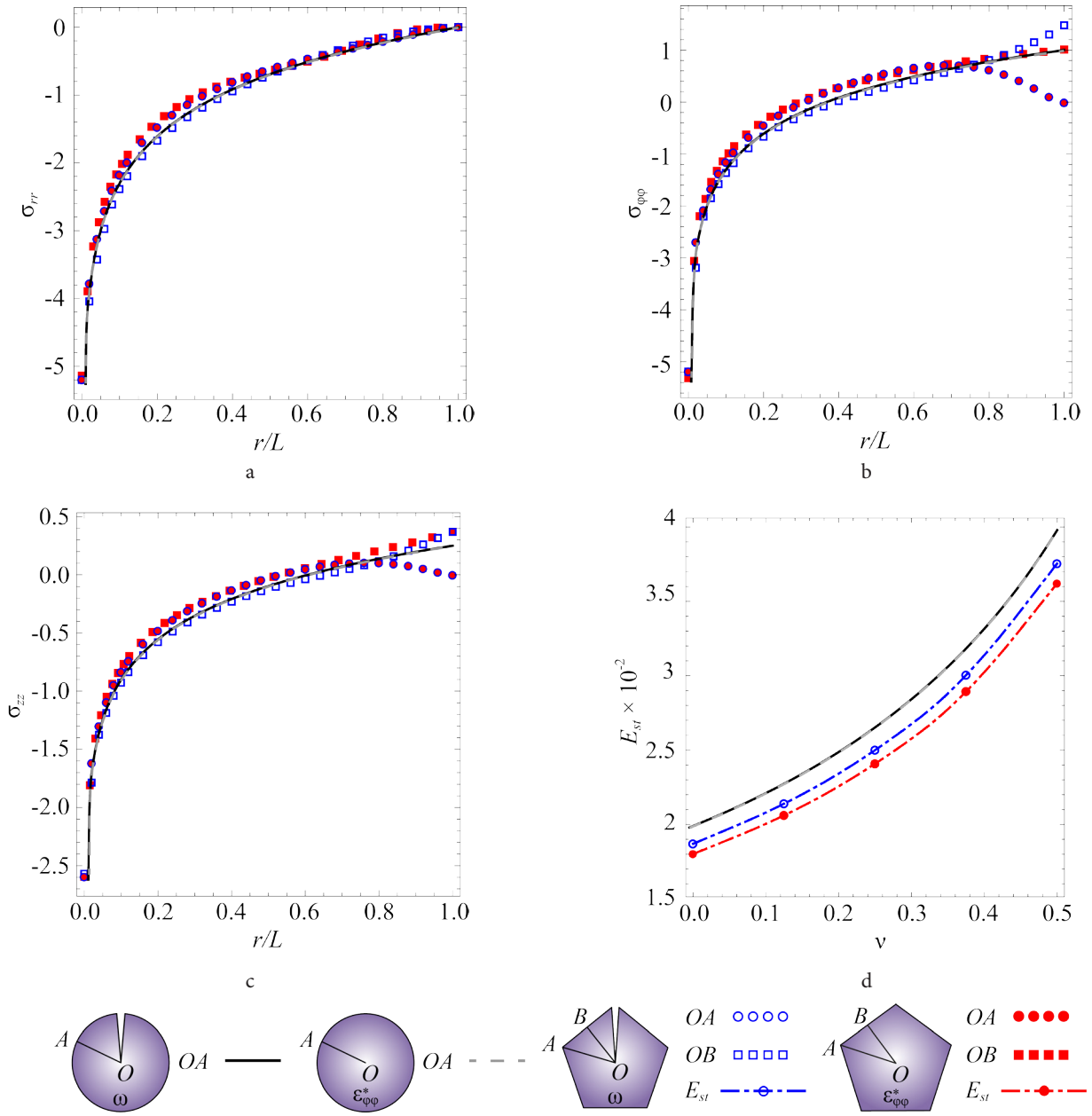

Fig. 4. (Color online) Dependencies of stress tensor components σ_{rr} (a), $\sigma_{\varphi\varphi}$ (b) and σ_{zz} (c) of a disclination defect on the ratio r/L ($L=R_0$ for the cylinder, $L=OA$ for the pentagon circumradius and $L=OB$ for the pentagon apothem) for $\nu=0.25$; the dependence of strain energy E_{st} on the Poisson ratio ν of the PW material (d). Stresses and energy are presented for the analytical solutions for single (solid curve) and distributed (dashed curve) disclination models, the FE solution (marks). The stresses are given in units $G\omega/[2\pi(1-\nu)]$ and the strain energy is given in units $G\omega^2R_0^2$.

ν increase. Besides, the strain energies obtained analytically take the largest values while FE ones take relatively low values. For example, for $\nu = 0.25$, the values $10^{-2}E_{st}/G\omega^2R_0^2$ are: ≈2.7 in the case of analytical solutions for WD and SD in the cylinder, ≈2.5 and ≈2.4 in the case of FE solutions for the pentagonal body containing WD and SD, respectively.

Cylindrical bodies containing either WD or SD were examined numerically by FE method as well. The discrepancy between the strain energies defined analytically and numerically (FE computations) has not been ascertained (the results of the modeling are not presented in this work). Therefore, it is the pentagonal shape that is responsible for the obtained discrepancy of strain energies between cylindrical and pentagonal bodies depicted in Fig. 4 d.

In our previous work [41], it was demonstrated that the strain energy of the cylindrical body containing a long prismatic inclusion with dilatational eigenstrain $\varepsilon^*_{xx} = \varepsilon^*_{yy} = \varepsilon^*_{zz}$ is proportional to the cross-section area of the inclusion and does not depend on the interface faceting. In the present work it is demonstrated that the strain energy of the PW subjected to the angular eigenstrain $\varepsilon^*_{\varphi\varphi}$ is strongly affected by the external faceting. Therefore, the internal interface in [41] is mainly responsible for the appearance of the coherent strained state in the core-shell wire, while the outer surface here is responsible for the elastic relaxation of the strained state in the PW.

5. Conclusions

A PW model was proposed to describe the internal stress in terms of stereo disclination with eigenstrain spread uniformly over the cylinder cross-section. A comparative analysis of the proposed distributed disclination model and the classical single disclination model of PWs was carried out using analytical calculations and FE modeling. It was shown that the elastic fields and strain energy were significantly affected by the PW distortion mode, considered either within single or distributed disclination approaches. The pentagonal faceting strongly impacts the elastic fields viz. stress reduction is observed in the vicinity of PW edges. As a result, the strain energy determined numerically for a pentagonal cross-section turns out to be lower than that determined analytically for a circular cross-section. The distributed disclination model seems to be preferable to the single disclination model in the case of FE modeling since the latter requires significantly more computational resources. Finally, it can be noted that FE modeling is applicable to describe the complex geometry of the PW to provide more accurate calculations. In contrast, analytical modeling is available for theoretical evaluations where high accuracy is not required.

References

1. J. Asselin, C. Boukouvala, E. R. Hopper, Q. M. Ramasse, J. S. Biggins, E. Ringe, Tents, Chairs, Tacos, Kites, and Rods: Shapes and Plasmonic Properties of Singly Twinned Magnesium Nanoparticles, ACS Nano 14 (2020) 5968 – 5980.
2. J. S. Du, W. Zhou, S. M. Rupich, C. A. Mirkin, Twin Pathways: Discerning the Origins of Multiply Twinned Colloidal Nanoparticles, Angew. Chem. 133 (2021) 6934 – 6939.
3. J. Bai, Y. Shi, W. Liang, C. Wang, Y. Liu, H. Wang, F. Liu, P. Sun, Y. Zhang, G. Lu, PtCu nanocrystals with crystalline control: Twin defect-driven enhancement of acetone sensing, Sens. Actuators B Chem. 354 (2022) 131210.
4. G. M. Argento, D. R. Judd, L. L. Etemad, M. M. Bechard, M. L. Personick, Plasmon-Mediated Reconfiguration of Twin Defect Structures in Silver Nanoparticles, J. Phys. Chem. C 127 (2023) 3890 – 3897.
5. E. Carbó-Argibay, B. Rodríguez-González, Controlled Growth of Colloidal Gold Nanoparticles: Single-Crystalline versus Multiply-twinned Particles, Isr. J. Chem. 56 (2016) 214 – 226.
6. H. Huang, A. Ruditskiy, S.-I. Choi, L. Zhang, J. Liu, Z. Ye, Y. Xia, One-Pot Synthesis of Penta-twinned Palladium Nanowires and Their Enhanced Electrocatalytic Properties, ACS Appl. Mater. Interfaces 9 (2017) 31203 – 31212.
7. M. Liu, Z. Lyu, Y. Zhang, R. Chen, M. Xie, Y. Xia, Twin-Directed Deposition of Pt on Pd Icosahedral Nanocrystals for Catalysts with Enhanced Activity and Durability toward Oxygen Reduction, Nano Lett. 21 (2021) 2248 – 2254.
8. J. Novák, P. Eliáš, S. Hasenöhrl, A. Laurenčíková, J. Kováč, jr, P. Urbancová, D. Pudiš, Twinned nanoparticle structures for surface enhanced Raman scattering, Appl. Surf. Sci. 528 (2020) 146548.
9. V. G. Gryaznov, A. M. Kaprelov, A. E. Romanov, I. A. Polonskii, Channels of Relaxation of Elastic Stresses in Pentagonal Nanoparticles, Phys. Status Solidi (b) 167 (1991) 441 – 450.
10. L. D. Marks, L. Peng, Nanoparticle shape, thermodynamics and kinetics, J. Phys.: Condens. Matter 28 (2016) 053001.
11. A. L. Kolesnikova, A. E. Romanov, Stress relaxation in pentagonal whiskers, Tech. Phys. Lett. 33 (2007) 886 – 888.
12. M. Yu. Gutkin, A. L. Kolesnikova, S. A. Krasnitckii, L. M. Dorogin, V. S. Serebryakova, A. A. Vikarchuk, A. E. Romanov, Stress relaxation in icosahedral small particles via generation of circular prismatic dislocation loops, Scripta Mater. 105 (2015) 10 – 13.
13. M. Yu. Krauchanka, S. A. Krasnitckii, M. Yu. Gutkin, A. L. Kolesnikova, A. E. Romanov, E. C. Aifantis, Generation of circular prismatic dislocation loops in decahedral small particles, Scripta Mater. 146 (2018) 77 – 81.
14. M. Yu. Krauchanka, S. A. Krasnitckii, M. Yu. Gutkin, A. L. Kolesnikova, A. E. Romanov, Circular loops of misfit dislocations in decahedral core-shell nanoparticles, Scripta Mater. 167 (2019) 81 – 85.
15. A. E. Romanov, I. A. Polonsky, V. G. Gryaznov, S. A. Nepijko, T. Junghanns, N. J. Vitrykhovski, Voids and channels in pentagonal crystals, J. Cryst. Growth 129 (1993) 691 – 698.
16. S. A. Krasnitckii, M. Yu. Gutkin, A. L. Kolesnikova, A. E. Romanov, Formation of a pore as stress relaxation mechanism in decahedral small particles, Lett. Mater. 12 (2022) 137 – 141.
17. A. S. Khramov, S. A. Krasnitckii, A. M. Smirnov,

M. Yu. Gutkin, The void evolution kinetics driven by residual stress in icosahedral particles, Mater. Phys. Mech. 50 (2022) 401–409.
18. A. S. Khramov, S. A. Krasnitckii, A. M. Smirnov, M. Yu. Gutkin, A kinetic model of the stress-induced void evolution in pentagonal whiskers and rods, Mater. Phys. Mech. 51 (2023) 22–33.
19. M. J. Walsh, K. Yoshida, A. Kuwabara, M. L. Pay, P. L. Gai, E. D. Boyes, On the Structural Origin of the Catalytic Properties of Inherently Strained Ultrasmall Decahedral Gold Nanoparticles, Nano Lett. 12 (2012) 2027–2031.
20. B. Goris, J. De Beenhouwer, A. De Backer, D. Zanaga, K. J. Batenburg, A. Sánchez-Iglesias, L. M. Liz-Marzán, S. Van Aert, S. Bals, J. Sijbers, G. Van Tendeloo, Measuring Lattice Strain in Three Dimensions through Electron Microscopy, Nano Lett. 15 (2015) 6996–7001.
21. W. Ji, W. Qi, X. Li, S. Zhao, S. Tang, H. Peng, S. Li, Investigation of disclinations in Marks decahedral Pd nanoparticles by aberration-corrected HRTEM, Mater. Lett. 152 (2015) 283–286.
22. R. de Wit, Partial disclinations, J. Phys. C: Solid State Phys. 5 (1972) 529–534.
23. A. Howie, L. D. Marks, Elastic strains and the energy balance for multiply twinned particles, Phil. Mag. A 49 (1984) 95–109.
24. A. E Romanov, A. L. Kolesnikova, Elasticity Boundary-Value Problems for Straight Wedge Disclinations. A Review on Methods and Results, Rev. Adv. Mat. Tech. 3 (2021) 55–95.
25. S. A. Krasnitckii, A. M. Smirnov, Pair interaction of intersecting dilatation and disclination defects, Condens. Matter Interphases 25 (2023) 505–513.
26. A. L. Kolesnikova, M. V. Dorogov, S. A. Krasnitckii, A. M. Smirnov, A. E. Romanov, Disclination models in the analysis of stored energy in icosahedral small particles, Mater. Phys. Mech. 51 (2023) 76–83.
27. Y. Ding, F. Fan, Z. Tian, Z. L. Wang, Atomic Structure of Au–Pd Bimetallic Alloyed Nanoparticles, JACS 132 (2010) 12480–12486.
28. Y. Ding, X. Sun, Z. L. Wang, S. Sun, Misfit dislocations in multimetallic core-shelled nanoparticles, Appl. Phys. Lett. 100 (2012) 111603.
29. S. Khanal, G. Casillas, N. Bhattarai, J. J. Velázquez-Salazar, U. Santiago, A. Ponce, S. Mejía-Rosales, M. José-Yacamán, CuS_2-Passivated Au-Core, Au_3Cu-Shell Nanoparticles Analyzed by Atomistic-Resolution Cs-Corrected STEM, Langmuir 29 (2013) 9231–9239.
30. S. Patala, L. D. Marks, M. Olvera de la Cruz, Elastic Strain Energy Effects in Faceted Decahedral Nanoparticles, J. Phys. Chem. C 117 (2013) 1485–1494.
31. S. Patala, L. D. Marks, M. Olvera de la Cruz, Thermodynamic Analysis of Multiply Twinned Particles: Surface Stress Effects, J. Phys. Chem. Lett. 4 (2013) 3089–3094.
32. A. I. Mikhailin, A. E. Romanov, Amorphization of disclination core, Solid State Physics. 28 (1986) 601–603. (in Russian)
33. K. Zhou, M. S. Wu, A. A. Nazarov, Relaxation of a disclinated tricrystalline nanowire, Acta Mater. 56 (2008) 5828–5836.
34. Y. Zhou, K. A. Fichthorn, Internal Stress-Induced Orthorhombic Phase in 5-Fold-Twinned Noble Metal Nanowires, J. Phys. Chem. C 118 (2014) 18746–18755.
35. D. Pohl, U. Wiesenhütter, E. Mohn, L. Schultz, B. Rellinghaus, Near-Surface Strain in Icosahedra of Binary Metallic Alloys: Segregational versus Intrinsic Effects, Nano Lett. 14 (2014) 1776–1784.
36. L. Deng, X. Liu, X. Zhang, L. Wang, W. Li, M. Song, J. Tang, H. Deng, S. Xiao, W. Hu, Intrinsic strain-induced segregation in multiply twinned Cu-Pt icosahedra, Phys. Chem. Chem. Phys. 21 (2019) 4802–4809.
37. R. T. Murzaev, A. A. Nazarov, Energies of formation and activation for migration of grain-boundary vacancies in a nickel bicrystal containing a disclination, Phys. Met. Metallogr. 102 (2006) 198–204.
38. A. A. Nazarov, Molecular dynamics simulation of the relaxation of a grain boundary disclination dipole under ultrasonic stresses, Lett. Mater. 6 (2016) 179–182.
39. A. E. Romanov, M. A. Rozhkov, A. L. Kolesnikova, Disclinations in polycrystalline graphene and pseudo-graphenes. Review, Lett. Mater. 8 (2018) 384–400.
40. M. A. Rozhkov, N. D. Abramenko, A. M. Smirnov, A. L. Kolesnikova, A. E. Romanov, Modelling of disclinated phosphorene crystals, Lett. Mater. 13 (2023) 45–49.
41. S. A. Krasnitckii, A. M. Smirnov, M. Yu. Gutkin, Misfit stress and energy in composite nanowire with polygonal core, Int. J. Eng. Sci. 193 (2023) 103959.